Obesity-dependent CDK1 signaling stimulates mitochondrial respiration at complex I in pancreatic β-cells

Received for publication, October 1, 2018, and in revised form, January 25, 2019 Published, Papers in Press, January 30, 2019, DOI 10.1074/jbc.RA118.006085

Trillian Gregg[‡1,2], **Sophia M. Sdao**[‡1], **Rashpal S. Dhillon**[§], **Jarred W. Rensvold**[¶], **Sophie L. Lewandowski**[‡], **David J. Pagliarini**[¶], **John M. Denu**[§], and **Matthew J. Merrins**[‡§‖3]

From the [‡]*Department of Medicine, Division of Endocrinology, Diabetes, and Metabolism and* [§]*Department of Biomolecular Chemistry, University of Wisconsin-Madison, Madison, Wisconsin 53705,* [¶]*Morgridge Institute for Research and Department of Biochemistry, University of Wisconsin-Madison, Madison, Wisconsin 53715, and* [‖]*William S. Middleton Memorial Veterans Hospital, Madison, Wisconsin 53705*

Edited by Jeffrey E. Pessin

β-Cell mitochondria play a central role in coupling glucose metabolism with insulin secretion. Here, we identified a metabolic function of cyclin-dependent kinase 1 (CDK1)/cyclin B1—the activation of mitochondrial respiratory complex I—that is active in quiescent adult β-cells and hyperactive in β-cells from obese (*ob*/*ob*) mice. In WT islets, respirometry revealed that 65% of complex I flux and 49% of state 3 respiration is sensitive to CDK1 inhibition. Islets from *ob*/*ob* mice expressed more cyclin B1 and exhibited a higher sensitivity to CDK1 blockade, which reduced complex I flux by 76% and state 3 respiration by 79%. The ensuing reduction in mitochondrial NADH utilization, measured with two-photon NAD(P)H fluorescence lifetime imaging (FLIM), was matched in the cytosol by a lag in citrate cycling, as shown with a FRET reporter targeted to β-cells. Moreover, time-resolved measurements revealed that in *ob*/*ob* islets, where complex I flux dominates respiration, CDK1 inhibition is sufficient to restrict the duty cycle of ATP/ADP and calcium oscillations, the parameter that dynamically encodes β-cell glucose sensing. Direct complex I inhibition with rotenone mimicked the restrictive effects of CDK1 inhibition on mitochondrial respiration, NADH turnover, ATP/ADP, and calcium influx. These findings identify complex I as a critical mediator of obesity-associated metabolic remodeling in β-cells and implicate CDK1 as a regulator of complex I that enhances β-cell glucose sensing.

In the field of islet biology, leptin-deficient (*ob*/*ob*) mice are a well-studied model for β-cell compensation arising from hyperphagia and obesity in which numerous adaptations to the insulin secretory pathway facilitate insulin hypersecretion, β-cell growth, and proliferation (1–4). In 2008, Attie and coworkers (5) took advantage of the phenotypic differences between lean (*i.e.* WT) and *ob*/*ob* mice to model the β-cell compensation and decompensation that accompanies type 2 diabetes. A strong genetic linkage was observed between the cell cycle regulators and diabetes susceptibility (5). Here, we focused on the potential significance of cyclin-dependent kinase 1 (CDK1)[4] and its activator, cyclin B1, for the β-cell secretory pathway.

CDK1/cyclin B1 signaling is essential for the control of proliferative signaling (6), and it was recently reported that CDK1 phosphorylates an estimated 52 mitochondrial substrates at CDK1 consensus sites, including eight subunits within complex I of the electron transport chain (7, 8). Complex I occupies a key position in the β-cell secretory pathway, by linking TCA cycle-dependent NADH turnover to the ATP/ADP ratio and membrane depolarization, the defining step of the β-cell triggering pathway (9). In addition, complex I is critical for the restoration of NAD^+/NADH required for glycolysis at glyceraldehyde-3-phosphate dehydrogenase. Apart from complex I, β-cells have few NADH redox disposals given the low levels of lactate dehydrogenase (which regenerates NAD^+) and the high levels of mitochondrial glycerol-3-phosphate dehydrogenase (which bypasses complex I), features that prevent β-cell glucose utilization from increasing under anaerobic contritions (*i.e.* the Pasteur effect) (10–12). An important question, then, is whether the insulin secretory pathway is impacted by CDK1 signaling, both in quiescent β-cells and during the adaptive response to obesity, when CDK1 signaling is up-regulated and insulin demand is high.

Here, we leveraged the small-molecule CDK1 inhibitor RO-3306 (13, 14) and direct complex I inhibition with rotenone to demonstrate that CDK1 signaling affects complex I to enhance oxidative phosphorylation in quiescent adult β-cells. We also show that obesity drives an increase in complex I flux in β-cells from *ob*/*ob* mice, where cyclin B1 mRNA and protein is

The work in the Merrins laboratory was supported by American Diabetes Association Grant 1-16-IBS-212; NIDDK, National Institutes of Health Grant R01DK113103; NIA, National Institutes of Health Grant R21AG050135; a New Investigator Award from the Wisconsin Partnership Program; and an Early Career Development Award from the Central Society for Clinical and Translational Research. The work in the Pagliarini laboratory was supported by NIDDK, National Institutes of Health Grant R01DK098672. The authors declare that they have no conflicts of interest with the contents of this article. The content is solely the responsibility of the authors and does not necessarily represent the official views of the National Institutes of Health.

[1] Both authors contributed equally to this work.

[2] Recipient of additional support from National Institutes of Health Molecular Biophysics Training Grant T32GM08293, the Laboratory for Optical and Computational Instrumentation, and a Wisconsin Alumni Research Foundation dissertation fellowship.

[3] To whom correspondence should be addressed: Medical Foundation Centennial Bldg., 1600 Overlook Terrace, Madison, WI 53705. Tel.: 608-256-1901 (ext. 12848); E-mail: merrins@wisc.edu.

[4] The abbreviations used are: CDK, cyclin-dependent kinase; FLIM, fluorescence lifetime imaging; TCA, tricarboxylic acid; Bis-Tris, 2-[bis(2-hydroxyethyl)amino]-2-(hydroxymethyl)propane-1,3-diol; DMEM, Dulbecco's modified Eagle's medium; ANOVA, analysis of variance.

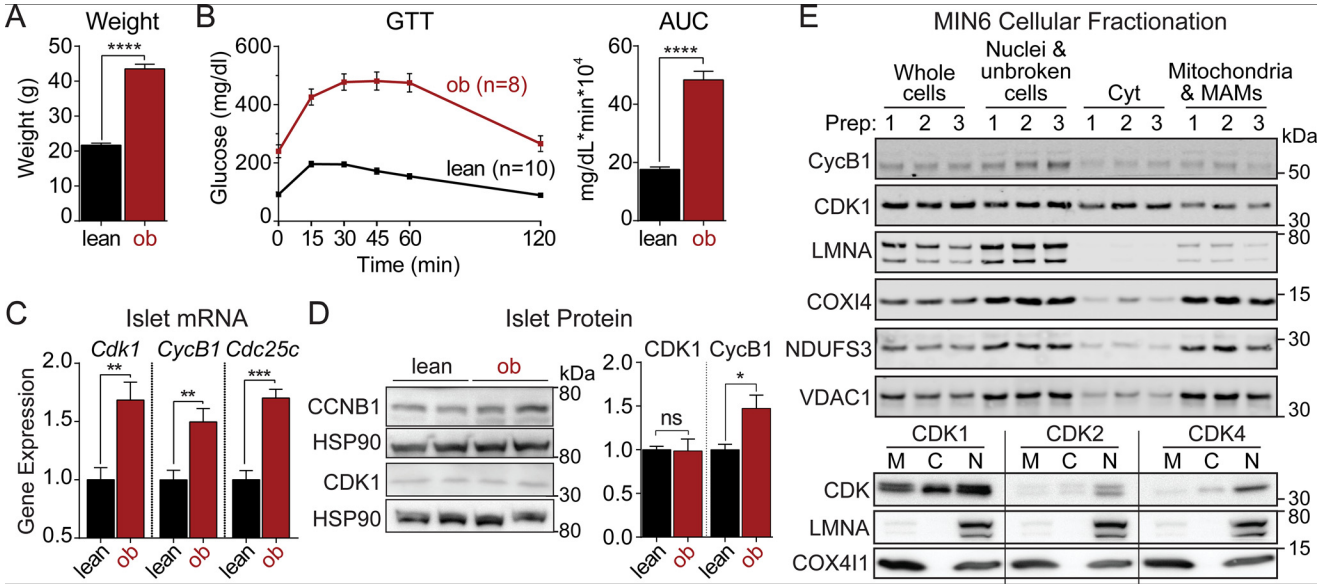

Figure 1. The CDK1 activator cyclin B1 is up-regulated in islets from obese (*ob*/*ob*) mice. Body weight (*A*) and intraperitoneal glucose tolerance test (*GTT*) (*B*) of lean (*i.e.* WT; $n = 10$) and *ob*/*ob* (*ob*; $n = 8$) mice aged 10–14 weeks were quantified as area under the curve (*AUC*). *C*, normalized islet gene expression in lean and *ob*/*ob* mice aged 10 weeks from Keller *et al.* (5) for *Cdk1*, cyclin B1/*Ccnb1* (*CycB1*), and *Cdc25c* ($n = 5$ mice per condition). *D*, Western blot of islet cyclin B1 and CDK1 from lean ($n = 8$) and *ob*/*ob* ($n = 9$) mice. Protein levels were quantified after normalizing to HSP90 loading controls. *E*, Western blots showing expression of cyclin B1 and CDK1 (*top*) or CDK1, CDK2, and CDK4 (*bottom*) together with mitochondrial (COX4I1, NDUFS33, and VDAC1) and nuclear (LMNA) markers following MIN6 cellular fractionation. Data are mean ± S.E. (*error bars*) and were compared by *t* test (*A* and *B*) or ANOVA with Sidak's post-test (*C* and *D*). *, $p < 0.05$; **, $p < 0.01$; ***, $p < 0.001$; ****, $p < 0.0001$; *ns*, not significant. *MAMs*, mitochondria-associated membranes; *Cyt*, cytoplasmic; *M*, mitochondrial; *C*, cytoplasmic; *N*, nuclear.

up-regulated. Suppression of complex I with CDK1 inhibition resulted in parallel reductions in NADH flux and cytosolic citrate cycling and, in *ob*/*ob* islets, imposed a further limitation on β-cell ATP/ADP and calcium influx. These studies identify a novel role for complex I in mediating the effects of obesity on the β-cell triggering pathway and implicate CDK1 signaling as the mechanism driving this effect.

Results

Cyclin B1 is up-regulated in pancreatic islets from obese (ob/ob) mice

Leptin-deficient obese (*ob*/*ob*) mice were used as a model of β-cell compensation (1–4). At 10 weeks of age, *ob*/*ob* mice weighed significantly more than their lean (*i.e.* WT) counterparts (Fig. 1*A*) and exhibited elevated fasting blood glucose and impaired glucose tolerance (Fig. 1*B*). We compared islet mRNA expression levels between lean and *ob*/*ob* mice using the database provided by Attie and co-workers (5) (http://diabetes.wisc.edu),[5] who previously described a confluence of gene expression changes surrounding the cell cycle regulators. Among these, the mRNA levels of *Cdk1* and its activators, cyclin B1 (*i.e. Ccnb1*) and *Cdc25c*, were increased in *ob*/*ob* mice relative to their lean counterparts (Fig. 1*C*). At the protein level, CDK1 was unchanged, whereas cyclin B1 was increased by 47% in *ob*/*ob* islets relative to lean controls (Fig. 1*D*).

CDK1 has been found in multiple cellular compartments, including a mitochondrial pool (7, 8, 15–17) and a cytosolic/nuclear pool (6). In MIN6 cells, significant amounts of cyclin B1 and CDK1 were found in the mitochondrial fraction, whereas CDK2 and CDK4 were more prominent in the nuclear fraction (Fig. 1*E*), suggesting a potential role of CDK1 in controlling β-cell mitochondrial function.

CDK1 activates mitochondrial respiration at complex I

Considering the established importance of mitochondrial CDK1 for complex I activation in other cell types (7, 8, 15), we hypothesized that the consequences of increased cyclin B1 in *ob*/*ob* islets would be enhanced CDK1 signaling and mitochondrial bioenergetics. To test this idea, we took advantage of the small-molecule CDK1 inhibitor RO-3306 (13, 14), which was chosen because its effectiveness to block CDK1-dependent complex I activation was previously validated with genetic mutants of CDK1, cyclin B1, and complex I (8). The dose and time course of RO-3306 application (5 μM; overnight preincubation) were chosen to match these studies. As an orthogonal approach, to test for and validate the CDK1 effects that are specific to complex I, CDK1 inhibition was compared with direct complex I inhibition with rotenone (0.001–5 μM; acute application).

To compare metabolic function in WT and *ob*/*ob* islets treated with CDK1 inhibitor, we performed multiphoton NAD(P)H fluorescence lifetime imaging (FLIM) using the assay we developed to assess NADH utilization by the electron transport chain in intact islets (18). Fig. 2*A* shows representative NAD(P)H lifetime images of WT and *ob*/*ob* islets stimulated with 10 mM glucose. These images are spatial maps of islet redox metabolism reflecting the distinct NAD(P)H lifetimes that accompany NADH and NADPH coenzyme binding to proteins (18, 19). Advantageously, much of the assay's resolution comes from NADH binding to complex I (20, 21), which was quantified by the phasor approach (22) as a shift along the $1 - g$

[5] Please note that the JBC is not responsible for the long-term archiving and maintenance of this site or any other third party hosted site.

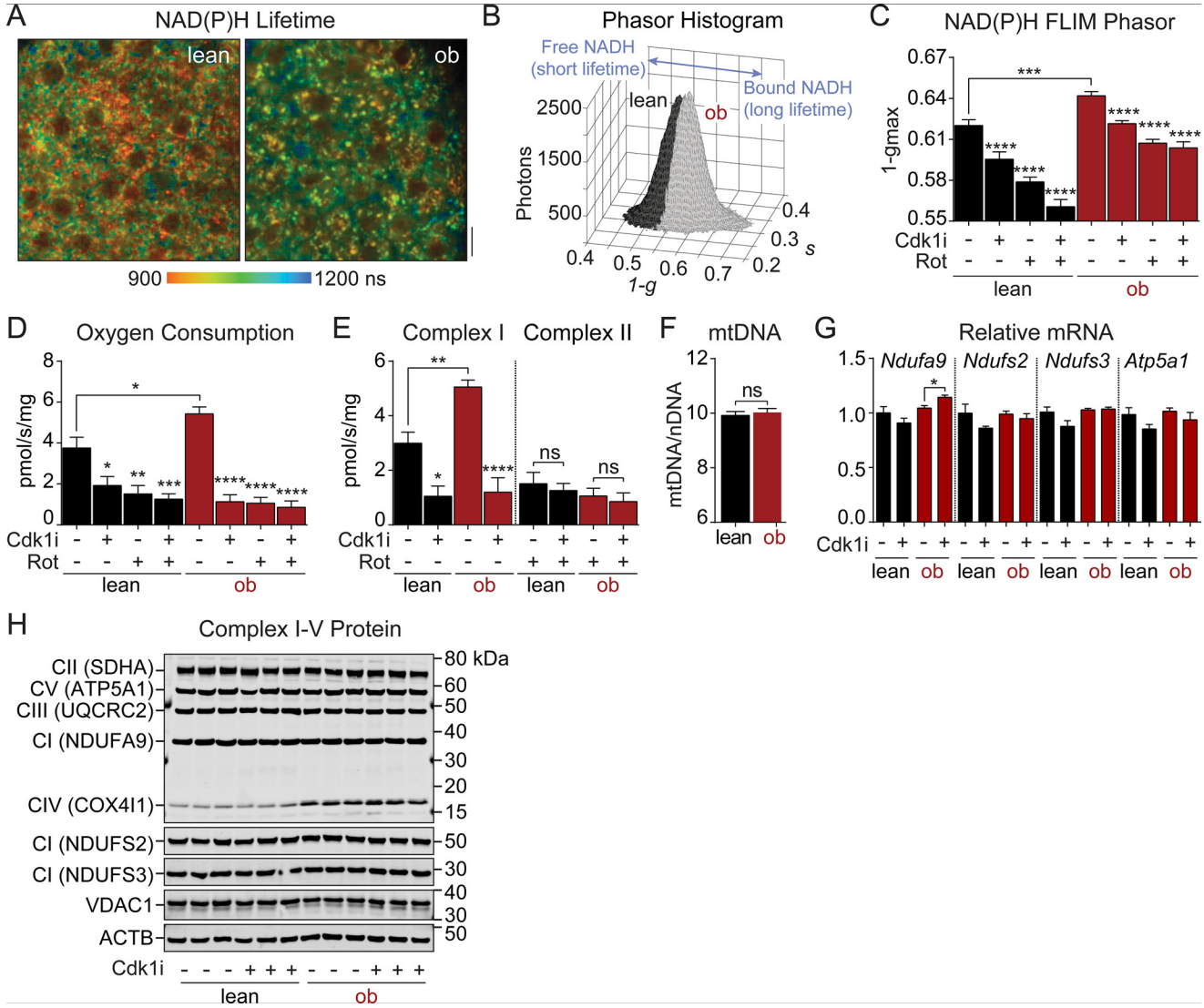

Figure 2. CDK1 increases mitochondrial NADH utilization by activating flux through complex I. *A*, representative multiphoton images showing the intensity-weighted mean NAD(P)H lifetime of lean and *ob*/*ob* islets imaged in 10 mM glucose. *Scale bar*, 5 μm. *B*, representative phasor histograms showing the frequency distribution of NAD(P)H lifetimes ($1 - g$, s) in lean ($n = 10$) and *ob*/*ob* ($n = 10$) islets imaged in 10 mM glucose. Projection of the phasor histogram peak along the abscissa (*C*) was used to quantify bound:free NAD(P)H in lean and *ob*/*ob* islets in the presence of 10 mM glucose, CDK1 inhibitor (*Cdk1i*) (5 μM RO-3306; 12 h), and complex I inhibitor (*Rot*) (5 μM rotenone; 15 min) as indicated ($n = 20$–22 islets per condition from two mice each). *D* and *E*, oxygen consumption rate of lean and *ob*/*ob* islets measured from five mice per condition (150 islets per mouse) with inhibitor treatments equivalent to *A*–*C*. Complex I and complex II fluxes during coupled state 3 respiration (*D*) are shown in *E*. *F*, mitochondrial mass in lean and *ob*/*ob* islets measured as the ratio of mitochondrial DNA (*mtDNA*) to nuclear DNA (*nDNA*) ($n = 3$ mice each). *G*, complex I (*Ndufa9*, *Ndufs2*, and *Ndufs3*) or complex V (*Atp5a1*) mRNA in WT islets treated with vehicle or CDK1 inhibitor (*Cdk1i*) (5 μM RO-3306; 12 h) ($n = 5$ mice each). *H*, protein levels of representative subunits from complexes I–V (*CI*–*CV*) and mitochondrial VDAC1 in lean and *ob*/*ob* islets treated with vehicle or CDK1 inhibitor (*Cdk1i*) (5 μM RO-3306; 12 h) with actin (*ACTB*) as a loading control ($n =$ 3 mice each, 100 islets/lane). Data are mean ± S.E. (*error bars*) and were compared by ANOVA with Sidak's post-test (*C*–*E*) or *t* test (*F* and *G*). *, $p < 0.05$; **, $p <$ 0.01; ***, $p < 0.001$; ****, $p < 0.0001$; *ns*, not significant.

axis (18). Relative to WT islets incubated in 10 mM glucose, the *ob*/*ob* islet phasor was shifted further along the $1 - g$ axis (Fig. 2, *B* and *C*), reflecting the increase in bound NADH lifetime that parallels complex I flux. As predicted, overnight incubation with CDK1 inhibitor (5 μM) reduced $1 - g_{max}$ in both WT and *ob*/*ob* islets, but to a lesser extent than direct complex I inhibition with rotenone (5 μM). The similar directionality of the two inhibitors in phasor space is consistent with CDK1 working on complex I. In *ob*/*ob* islets, the simultaneous application of these inhibitors had no further effect, implying that the electron transport chain in *ob*/*ob* islets is more highly dependent on CDK1 signaling relative to WT controls.

To directly test the effect of CDK1 inhibition on individual electron transport chain fluxes, we measured oxygen consumption in permeabilized mouse islets stimulated with mitochondrial fuels for complex I (glutamate and malate) and complex II (succinate). In excellent agreement with the NAD(P)H FLIM assay, *ob*/*ob* islets exhibited increased state 3 respiration relative to lean controls, and complex I flux was restricted by overnight application of CDK1 inhibitor (Fig. 2, *D* and *E*). No further effect of CDK1 inhibition was seen when complex I was directly inhibited with rotenone. Compared with WT islets, the elevated cyclin B1 levels observed in *ob*/*ob* islets (Fig. 1) would be predicted to activate CDK1 signaling and stimulate complex I

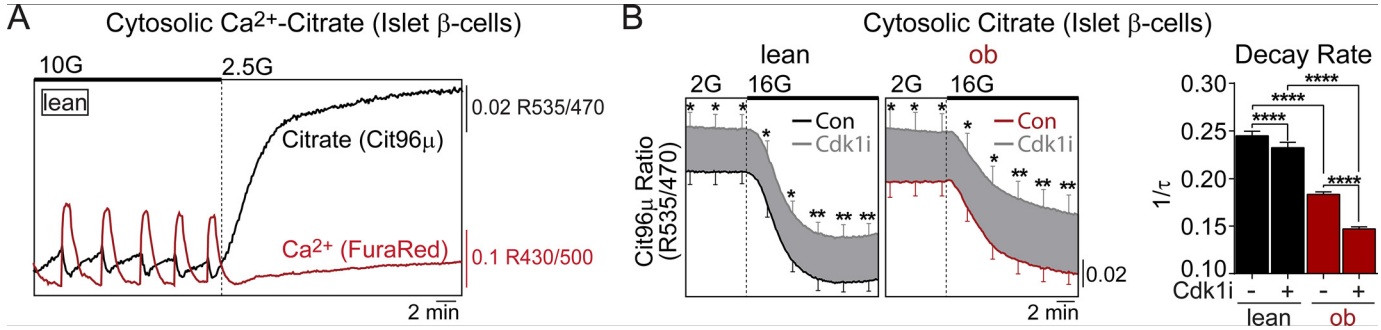

Figure 3. CDK1 blockade restricts cytosolic citrate cycling in islet β-cells. *A*, representative simultaneous measurement of cytosolic citrate and calcium in WT islet β-cells. *B*, measurements of cytosolic citrate in islet β-cells from lean and *ob*/*ob* mice after overnight pretreatment with vehicle (0.1% DMSO) or CDK1 inhibitor (*Cdk1i*) (5 μM RO-3306; 12 h). The response to glucose elevation from 2 to 16 mM was quantified by the decay rate ($1/\tau$) of cytosolic citrate levels. n = 61–66 WT islets and n = 30–34 *ob*/*ob* islets per condition from three mice of each genotype. *Error bars* are shown every 3 min for clarity. Data are mean ± S.E. (*error bars*) and were compared by ANOVA with Sidak's post-test. *2G*, 2 mM glucose; *10G*, 10 mM glucose. *, $p < 0.05$; **, $p < 0.01$; ****, $p < 0.0001$.

in turn. As expected, respiration in *ob*/*ob* islets exhibited higher rotenone sensitivity than lean controls (84 ± 6% reduction in *ob*/*ob versus* 61 ± 11% in WT, $n = 5$, $p < 0.0001$). CDK1 inhibition had no acute effect on respiration, NAD(P)H, or Ca^{2+} oscillations (data not shown), which is consistent with prior studies (8) and rules out off-target inhibition of complex I by RO-3306. Complex II flux, which was comparable between WT and *ob*/*ob* islets, was unaffected by treatment with CDK1 inhibitor (Fig. 2*E*). No changes in mitochondrial number were observed between strains (Fig. 2*F*), and no changes in complex I gene expression (Fig. 2*G*) or complex I–V protein expression (Fig. 2*H*) were observed in response to the CDK1 inhibitor pretreatment. Taken together, the NAD(P)H FLIM and respirometry experiments demonstrate that complex I is more active in *ob*/*ob* than WT islets and identify complex I as a target of CDK1 signaling in islets.

CDK1 blockade slows glucose-dependent citrate cycling

It is well known that glucose utilization in β-cells does not accelerate under anaerobic conditions (the Pasteur effect), facilitating a tight bidirectional coupling between cytosolic and mitochondrial fluxes (12). To confirm that the brake on NADH and electron transport chain fluxes induced by CDK1 blockade is propagated to the cytosol, we focused on cytosolic citrate, a critical signaling intermediate produced by the mitochondria in response to glucose (23–26). To assess the cytosolic citrate levels specifically in islet β-cells, we used a FRET-based citrate sensor (27) driven by the insulin promoter (28). In response to 10 mM glucose, steady-state oscillations in citrate were out of phase with cytosolic Ca^{2+}, measured simultaneously, and glucose depletion was accompanied by a rise in citrate (Fig. 3*A*). Thus, although citrate is produced and transported from the mitochondria at higher rates in response to glucose (23, 24), it is depleted at a higher rate in the cytosol, likely to meet NADPH demand through the actions of isocitrate dehydrogenase and malic enzyme (25). Although this assay is agnostic to the particular fate of citrate, the cytosolic citrate level is metabolically dependent and is therefore suitable to test whether CDK1 inhibition affects cytosolic fluxes. In response to glucose elevation, cytosolic citrate levels fell sharply in both WT and *ob*/*ob* β-cells, and the relative concentration of citrate (proxied by the FRET ratio) was increased by overnight treatment with CDK1 inhibitor in both genotypes (Fig. 3*B*). Relative to WT β-cells, the citrate decay rate in *ob*/*ob* β-cells was more sensitive to CDK1 inhibition (Fig. 3*C*), which was also the case with NADH utilization and flux through complex I (Fig. 2).

Complex I inhibition, with CDK1 blockade or rotenone, restricts β-cell ATP/ADP cycling and calcium influx in ob/ob islets

In the β-cell triggering pathway, the metabolism-dependent rise in ATP/ADP is used sequentially to stimulate K_{ATP} channel closure, Ca^{2+} influx, and insulin secretion. To assess the control of this pathway by CDK1, we simultaneously examined the cytosolic ATP/ADP and calcium oscillations that transmit the encoded signals generated by glucose metabolism to the exocytotic machinery. Steady-state Ca^{2+} oscillations were assessed in WT and *ob*/*ob* islets preincubated with vehicle or CDK1 inhibitor (Fig. 4, *A* and *B*). We then quantified the oscillatory duty cycle, the fraction of time spent in the active state during each oscillation, and the glucose-encoded parameter that defines the β-cell triggering pathway (18, 29, 30). Consistent with an increased sensitivity to glucose, *ob*/*ob* islets stimulated by 8 mM glucose exhibited a higher duty cycle than WT islets stimulated by 10 mM glucose. Treatment with CDK1 inhibitor had no effect on the duty cycle of β-cell ATP/ADP or calcium oscillations in WT islets (Fig. 4*A*) but induced a parallel reduction in both parameters in *ob*/*ob* islets ($p < 0.001$) (Fig. 4*B*).

If CDK1 acts via complex I to alter calcium influx, then the application of rotenone would be expected to match the effect of CDK1 inhibition on the calcium duty cycle. In WT islets or *ob*/*ob* islets, high doses of rotenone (≥100 nM) blocked the ability of β-cells to maintain ATP/ADP and terminated metabolic and calcium oscillations (Fig. 5, *A–D*). At concentrations <100 nM rotenone, dynamic cross-talk between metabolism and the plasma membrane persisted, and the effects of complex I inhibition were analyzed from the duty cycle of ATP/ADP and calcium oscillations. A clear defect in β-cell glucose sensing was quantified from the reduced ATP/ADP oscillation duty cycle in the presence of low-dose rotenone (10 nM), with the magnitude of the decrease being greater in *ob*/*ob* than WT islets (Fig. 5, *A* and *C*). These effects were matched by the calcium duty cycle, measured in separate experiments (Fig. 5, *B* and *D*).

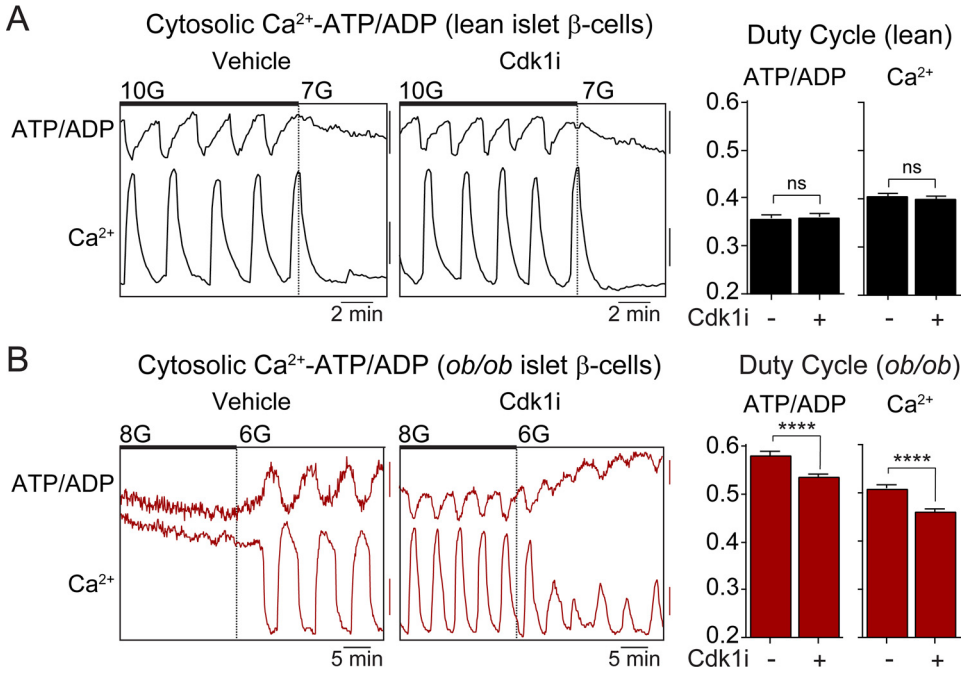

Figure 4. CDK1 blockade restricts β-cell ATP/ADP and Ca^{2+} influx in *ob/ob* islets. *A* and *B*, Ca^{2+} oscillations in lean (*A*) and *ob/ob* (*B*) islets in the presence of 6–10 mM glucose as indicated. The islets were pretreated with 0.1% DMSO (*Con*) or CDK1 inhibitor (*Cdk1i*) (5 μM RO-3306; 12 h) as indicated. The duty cycle at 10 mM glucose (lean; *A*) and 8 mM glucose (*ob/ob*; *B*) was calculated as the fraction of time spent in the active state of each oscillation, defined as >50% oscillation amplitude. Lean ATP/ADP, $n = 119–132$ islets from three mice; lean calcium, $n = 178–168$ islets from six mice; *ob/ob* ATP/ADP, $n = 99–102$ islets from three mice; *ob/ob* calcium, $n = 151–164$ islets from six mice. *Scale bar*, lean ATP/ADP, 0.01 R500/430; lean calcium, 0.05 R430/500; *ob/ob* ATP/ADP, 5 arbitrary units; *ob/ob* calcium, 0.025 R430/500. Data are mean ± S.E. (*error bars*) and were compared by *t* test. *10G*, 10 mM glucose; *7G*, 7 mM glucose. **** $p <$ 0.0001; *ns*, not significant.

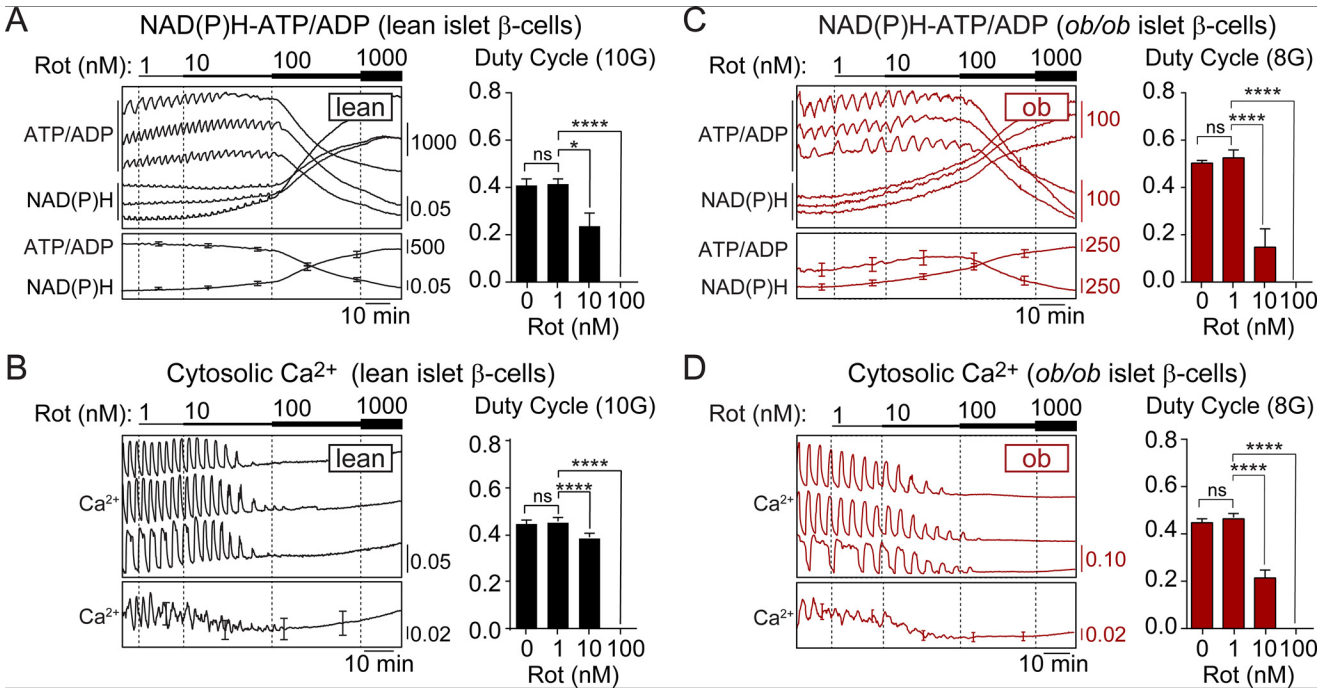

Figure 5. Low-dose rotenone mimics the restrictive effect of CDK1 inhibitor on Ca^{2+} influx. *A–D*, response of glucose-stimulated NAD(P)H, ATP/ADP, and Ca^{2+} oscillations in WT islets ($n = 23$) exposed to 10 mM glucose (*A* and *B*) and *ob/ob* islets ($n = 26$) exposed to 8 mM glucose (*C* and *D*) to increasing concentrations of rotenone (*Rot*) (1–1000 nM as indicated). The calcium duty cycle at each dose of rotenone was calculated as the fraction of time spent in the active state of each oscillation, defined as >50% oscillation amplitude. Data are mean ± S.E. (*error bars*) and were compared by ANOVA with Sidak's post-test. *, $p < 0.05$; ****, $p < 0.0001$; *ns*, not significant.

Taken together with the identification of complex I as a target of CDK1 (Fig. 2), the matching effects of CDK1 inhibitor and rotenone strongly imply that the influence of CDK1 on β-cell calcium dynamics is mediated by its activating effect on complex I. The heightened reliance of *ob/ob* islets on complex I for respiration further explains why CDK1 and rotenone exert

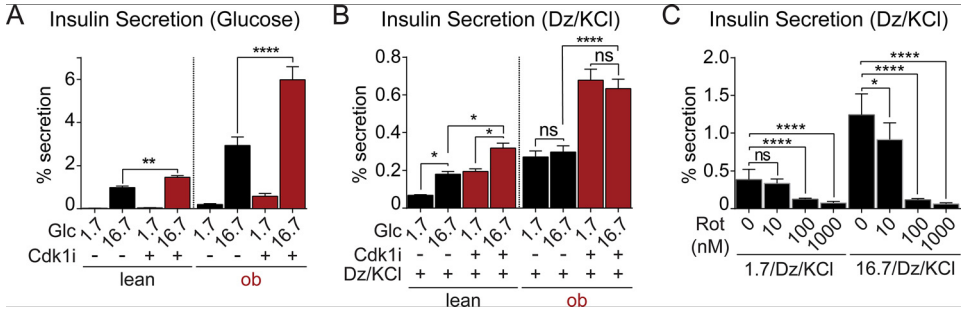

Figure 6. CDK1 inhibits insulin secretion independently of metabolism. *A*, *ex vivo* glucose-stimulated insulin secretion normalized to insulin content in islets isolated from lean ($n = 3$) and *ob*/*ob* ($n = 3$) mice. Islets were pretreated with vehicle (0.1% DMSO) or CDK1 inhibitor (*Cdk1i*) (5 μM RO-3306; 12 h). *B*, K_{ATP} channel–independent insulin secretion normalized to insulin content in islets isolated from lean ($n = 3$) and *ob*/*ob* ($n = 3$) mice in the presence of 30 mM KCl, 200 μM diazoxide (*Dz*), and 1.7 or 16.7 mM glucose (*Glc*). Islets were pretreated with vehicle or CDK1 inhibitor (*Cdk1i*) (5 μM RO-3306; 12 h). *C*, K_{ATP} channel–independent insulin secretion normalized to insulin content in WT islets ($n = 3$ mice) in the presence of increasing concentrations of rotenone. No difference in insulin content was observed between groups (not shown). Data are mean ± S.E. (*error bars*) and were compared by ANOVA with Sidak's post-test. *, $p < 0.05$; **, $p < 0.01$; ****, $p < 0.0001$; *ns*, not significant.

more control over ATP/ADP and calcium in *ob*/*ob* islets than in WT controls.

CDK1 blockade enhances insulin secretion independently of metabolism

We then tested the effects of CDK1 inhibition on glucose-stimulated insulin secretion using islets isolated from WT and *ob*/*ob* mice (Fig. 6*A*). Insulin secretion stimulated by 16.7 mM glucose was increased by CDK1 blockade with RO-3306, by 48 ± 13% in WT islets ($p < 0.01$) and 104 ± 32% in *ob*/*ob* islets ($p < 0.0001$), where insulin secretion was initially higher. Insulin content was unaffected by CDK1 inhibition in either WT or *ob*/*ob* islets (not shown). These results demonstrate that the inhibition of β-cell calcium by CDK1 blockade is not the dominant effect on insulin secretion.

To determine whether CDK1 inhibitor affects depolarization-induced insulin secretion, islets were exposed to 1.7 or 16.7 mM glucose in the continuous presence of 200 μM diazoxide (to open K_{ATP} channels) and 30 mM KCl (to depolarize the plasma membrane). CDK1 inhibitor approximately doubled the K_{ATP}-independent secretory capacity in all treatments, with the enhancement of secretion at 1.7 mM glucose indicating a metabolism-independent effect of CDK1 inhibition (Fig. 6*B*). As a further test that complex I is uninvolved in this effect, we compared the effect of CDK1 inhibitor with direct complex I inhibition with rotenone using the same secretion assay. At no point was insulin secretion augmented by rotenone; at both 1.7 and 16.7 mM glucose, KCl-stimulated insulin secretion was dose-dependently reduced by rotenone over the concentration range of 10–1000 nM (Fig. 6*C*). No differences in insulin content were observed in response to CDK1 inhibitor or rotenone (not shown). These data suggest that CDK1 has secondary targets that affect the exocytotic machinery.

Discussion

Here, we demonstrate that CDK1 signaling is required for full complex I activity in quiescent β-cells. Through this mechanism, CDK1 was found to exert control over mitochondrial respiration, NADH utilization, and citrate cycling. In *ob*/*ob* islets, CDK1 blockade induced a further limitation on ATP/ADP and calcium influx, which is likely explained by higher cyclin B1 levels and the heightened reliance of *ob*/*ob* islets on complex I for respiration. Apart from insulin secretion, which was altered by CDK1 inhibition independently of metabolism, direct complex I inhibition with rotenone matched the effects of CDK1 inhibitor on mitochondrial respiration, NADH utilization, and calcium influx. These studies reveal a novel role for CDK1 in controlling mitochondrial complex I in quiescent β-cells and identify CDK1 and complex I as critical mediators of obesity-dependent remodeling of the β-cell triggering pathway.

Control of islet respiration by CDK1 in WT islets, although similar to studies in non-β-cells (8), is much stronger in *ob*/*ob* islets. In WT islets, CDK1 inhibition reduced complex I flux by 65% and state 3 respiration by 49%, compared with 76% of complex I flux and 79% of state 3 respiration in *ob*/*ob* islets, minimizing the ability of complex II to compensate for CDK1 blockade in *ob*/*ob* islets. To discern the effects of respiration on the triggering pathway, we focused on the calcium duty cycle, the fraction of time spent in the active state of an oscillation, and the mechanism by which glucose sensing is encoded in β-cell metabolic and electrical oscillations (30). Based on the glucose dependence of the calcium duty cycle (18), it can be estimated that activating CDK1 in *ob*/*ob* islets has the same effect as increasing extracellular glucose by 1.6 mM. Importantly, CDK1 blockade in *ob*/*ob* islets normalized respiration to WT levels, although calcium influx was not completely restored, indicating the presence of additional compensatory mechanisms controlling the triggering pathway.

We propose that there are two key functions of complex I activation by CDK1 in β-cells beyond the ATP production required for the high bioenergetic demands of insulin biosynthesis, the maintenance of ionic gradients, and exocytosis (31, 32). The first is redox disposal, *i.e.* restoring the cytosolic NAD^+ required to run glycolysis at GAPDH. Complex I is likely rate-limiting for NAD^+ regeneration because β-cells lack the Pasteur effect due to the low level of the NAD^+-generating enzyme lactate dehydrogenase (11, 33) and the high level of mitochondrial glycerol 3-phosphate dehydrogenase, which bypasses complex I by shuttling electrons into complex II (10). The second is that complex I is important for the metabolic amplification of insulin secretion, which was dose-dependently blocked by rotenone. Many of the proposed amplifying pathways depend on the buildup of TCA cycle intermediates

(anaplerosis) and their egress from the mitochondria (cataplerosis) (23, 24). Citrate exiting the mitochondrial TCA cycle can produce NADPH at isocitrate dehydrogenase (25) or be processed by ATP citrate lyase to produce oxaloacetate and acetyl-CoA (ultimately amplifying insulin secretion through malonyl-CoA) (9). A full turn of the citrate–pyruvate cycle can also generate NADPH at malic enzyme, or malate can reenter the mitochondria and shunt the TCA cycle, entering the phosphoenolpyruvate cycle, which stimulates insulin secretion by an unknown mechanism (26, 34). Consistent with these functions of complex I, CDK1 inhibition was found to reduce cytosolic citrate cycling.

The importance of CDK1 signaling to islet respiration is consistent with prior studies showing that mitochondrial CDK1 directly phosphorylates complex I (7, 8, 15). In these studies, RO-3306 and phosphorylation-insensitive mutants of complex I were shown to block the effects of CDK1/cyclin B1 on oxidative phosphorylation (8). In support of a post-translational mechanism in β-cells, CDK1 inhibition had no effect on complex I mRNA or protein levels in WT or *ob*/*ob* islets. However, as we were unable to detect any of the eight CDK1 substrates on complex I (8) by phosphoproteomics (despite identifying >30,000 sites in MIN6 cells), our study does not address whether CDK1 acts via complex I phosphorylation; the effects of RO-3306 could be indirect or involve cytosolic/nuclear CDK1 signaling, such as the recently discovered FOXM1/PLK1/CENP-A pathway (35). A further limitation of our study is the lack of genetic evidence for the control of complex I by CDK1. Our efforts to delete CDK1 were frustrated by the embryonic lethality of mice lacking β-cell CDK1 (CDK1-floxed mice (36); Ins1-Cre mice (37)) and by the inefficacy of Ins1-CreER mice (Jax 026802) (37) to catalyze *loxP* excision. Inconsistent outcomes with Ins1-CreER mice are becoming widely known,[6] although there are published successes (38). Even so, direct complex I inhibition with rotenone mimicked the effect of CDK1 inhibition on islet respiration, NADH utilization, ATP/ADP, and calcium influx.

In conclusion, we have elucidated a novel mechanism by which CDK1 exerts control over the threshold for β-cell calcium influx in obese animals. To date, all cyclin-dependent kinases tested have essential roles in β-cell glucose sensing, some in quiescent β-cells (39, 40). By highlighting the noncanonical functions of cyclin-dependent kinases, these studies further our understanding of the linkage between proliferative signaling and energy metabolism (41) and inform type 2 diabetes therapies that target proliferative signaling.

Experimental procedures

Mice

All animal studies were approved by the Institutional Animal Care and Use Committees of the University of Wisconsin-Madison and the William S. Middleton Memorial Veterans Hospital. C57Bl6/J WT and leptin-deficient (*ob*/*ob*) mice were obtained from The Jackson Laboratory (stocks 000664 and 000632). Male mice were analyzed between 10 and 16 weeks of age.

[6] C. Evans-Molina, J. Johnson, D. Scott, and C. Wright, personal communications.

In vivo studies

Glucose tolerance tests were performed on mice fasted overnight for 16 h. Following intraperitoneal injection of 1 g/kg glucose in sterile saline, glucose measurements were obtained via tail nick using a Bayer Contour glucometer at 0, 15, 30, 60, and 120 min postinjection.

Islet isolation and CDK1 inhibitor treatment

Mice were sacrificed via cervical dislocation, and islet isolations were carried out as described previously (18). Islets were cultured overnight in RPMI 1640 medium supplemented with 10% (v/v) fetal bovine serum (Invitrogen, A31605), 100 units/ml penicillin, and 100 μg/ml streptomycin (Invitrogen) containing vehicle (0.1% DMSO) or CDK1 inhibitor, 5 μM RO-3306 (Enzo, ALX-270-463) (13).

Cell fractionation

MIN6 cells grown on 10-cm plates were washed twice with 5 ml of cold Dulbecco's PBS (Thermo, 14190144) while on ice. Cells were removed from plates via scraping in 1 ml of Dulbecco's PBS containing a protease inhibitor mixture (Sigma, 4693159001), transferred to 15-ml conical tubes, and pelleted at 3000 × *g* for 5 min at 4 °C. Three plates of cells were used for each fractionation replicate and combined after scraping. Cell pellets were resuspended in 500 μl of hypotonic buffer (20 mM Tris, 1 mM EDTA (pH 7.4)) and incubated on ice for 30 min. Protease inhibitors (pepstatin A, chymostatin, antipain, leupeptin, and aprotinin) were added to a concentration of 0.5 μg/ml each, and phosphatase inhibitors were added (500 μM imidazole, 250 μM NaF, 300 μM sodium molybdate, 250 μM sodium orthovanadate, and 1 mM sodium tartrate). Sodium butyrate was added to a final concentration of 5 mM. Cells were homogenized with a 1-ml glass Dounce grinder and tight-fitting pestle (Wheaton, 357538) using 40 strokes. Then 500 μl of a sucrose/mannitol solution (440 mM mannitol, 140 mM sucrose, 20 mM Tris (pH 7.4), 1 mM EDTA) was added, and samples were centrifuged at 700 × *g* for 10 min at 4 °C. The supernatant was transferred to a new tube and centrifuged at 12,000 × *g* for 10 min at 4 °C. Samples of the input (whole cell) and slow-centrifugation supernatant fraction (cytoplasm) were taken during the procedure. The slow- (nuclei/unbroken cells) and fast (mitochondria/mitochondria-associated membranes)-centrifugation pellets were solubilized in radioimmune precipitation assay buffer, and 8 μg of each fraction, as determined by BCA assay, was analyzed via immunoblotting as described above.

Immunoblotting

Protein lysates from isolated islets were prepared in 20 mM Tris, 100 mM NaCl, 1 mM EDTA, 0.5% Triton X-100 or radioimmune precipitation assay buffer composed of 150 mM NaCl, 1% IGEPAL CA-630, 0.5% sodium deoxycholate, 0.1% SDS, 50 mM Tris (pH 8.0), 0.4 mM EDTA (pH 8.0), 10% glycerol, and a protease inhibitor mixture (Millipore Sigma, 11836170001). Then 15 μg of cleared lysate, as determined by BCA assay (Thermo, 23225) or Pierce 660 nm protein assay (Thermo Fisher), was separated on a 4–12% Bis-Tris Gel (Invitrogen,

NP0323BOX) with a protein standard (Invitrogen, LC5800), transferred to polyvinylidene difluoride (Millipore Sigma, IPFL00010), probed with primary antibodies, and analyzed using a LI-COR Odyssey CLx Imaging System with secondary antibodies (LI-COR Biosciences, 925-32210, 926-32211, 926-68070, and 926-68071). Primary antibodies used were: actin (ACTB) (Abcam, ab8224; 1:2000), CCNB1 (Cell Signaling Technology, 4138S; 1:1000), CDK1 (Cell Signaling Technology, 77055S; 1:1000), CDK4 (Santa Cruz Biotechnology, sc260; 1:1000), COX4I1 (Cell Signaling Technology, 11967S; 1:500), HSP90 (Cell Signaling Technology, 4877S; 1:1000), NDUFS2 (Abcam, ab192022; 1:1000), NDUFS3 (Abcam, ab14711; 1:1000), VDAC1 (Abcam, ab18988), and OXPHOS Blue Native WB Mixture (ATP5A1, COX4I1, NDUFA9, SDHA, and UQCRC2; Abcam, ab110412; 1:500).

Cloning and adenoviral delivery of citrate biosensors into islet β-cells

The cDNA for the citrate biosensor (Cit96μ; K_d = 96 μM) (27) was synthesized using gBlocks (Integrated DNA Technologies, Inc.) and cloned by Gibson assembly (New England Biolabs) into a modified pENTR-DS shuttle vector (Invitrogen) containing the rat insulin promoter (RIP) as in a previous study (42). Clonase II/Gateway (Invitrogen) was then used to prepare the full-length adenoviral construct in pAd/PL-DEST (Invitrogen), yielding β-cell–specific citrate biosensors (pAd-PL-RIP1-Cit96μ-pA). Islets were infected immediately postisolation with 2 μl of high-titer adenovirus for 2 h at 37 °C and then moved to fresh medium overnight.

Biosensor imaging

Islets treated with vehicle or CDK1 inhibitor were imaged simultaneously; one treatment group was prelabeled with 0.5 μg/ml DiR (Molecular Probes, D12731) for 10 min. DiR labeling had no effect on islet metabolic or Ca^{2+} oscillations (data not shown). For measurements of cytosolic Ca^{2+}, islets were preincubated in 2.5 μM FuraRed (Molecular Probes, F3020) in islet medium for 45 min at 37 °C. Islets were imaged in a glass-bottomed imaging chamber (Warner Instruments) mounted on a Nikon Ti-Eclipse inverted microscope equipped with a 20×/0.75 numerical aperture SuperFluor objective (Nikon Instruments). The chamber was perfused with a standard external solution containing 135 mM NaCl, 4.8 mM KCl, 2.5 mM $CaCl_2$, 1.2 mM $MgCl_2$, 20 mM HEPES (pH 7.35). The flow rate was 0.4 ml/min, and temperature was maintained at 33 °C using solution and chamber heaters (Warner Instruments). Excitation was provided by a SOLA SEII 365 (Lumencor) set to 10% output. Single DiR images utilized a Chroma Cy7 cube (710/75x, T760lpxr, 810/90m). Excitation (x) or emission (m) filters (ET type; Chroma Technology) were used in combination with an FF444/521/608-Di01 dichroic beamsplitter (Semrock) as follows: FuraRed, 430/20x and 500/20x, 630/70m (R430/500); NAD(P)H, 365/20x, 470/24m; citrate, 430/20x and 500/20x, 535/35m (R500/430); and Perceval-HR, 430/20x and 500/20x, 535/35m (R500/430). Fluorescence emission was collected with a Hamamatsu ORCA-Flash4.0 V2 Digital CMOS camera every 6 s. A single region of interest was used to quantify the average response of each islet using Nikon Elements and custom MATLAB software (MathWorks).

NAD(P)H fluorescence lifetime imaging

Islets were imaged in number 1.5 glass-bottom dishes on a custom-built multiphoton laser-scanning system based around a Nikon TE-300 inverted microscope equipped with a PlanApo 60×/1.4 numerical aperture oil immersion objective (Nikon Instruments) in a standard external solution (above). Temperature was maintained at 35 °C using a LiveCell incubator (Pathology Devices). NAD(P)H was excited with a Mai Tai DeepSee Ti:sapphire laser (Spectra-Physics) at 740 nm with a 450/70m bandpass emission filter (Chroma) before collection by a Hamamatsu H7422P-40 GaAsP photomultiplier tube. FLIM images were collected at 256 × 256 resolution with 120-s collection at 1 Hz using SPC-830 Time-Correlated Single Photon Counting (TCSPC) electronics (Becker & Hickl GbmH). In each experiment, urea crystals were used to define the instrument response function with a 370/10m bandpass emission filter (Chroma), and coumarin was used as a reference for lifetime (2.5 ns) using a 450/70m bandpass emission filter (Chroma). For analysis, raw SDT files were imported into MATLAB (MathWorks), and a custom script was used to generate phasor histograms for each treatment using the equations in Digman *et al.* (22). All data were reported as the phasor histogram peak ($1 - g_{max}$, s_{max}).

Islet respirometry

Following overnight incubation, 150 islets/condition/mouse (five mice/condition) were transferred to a 35-mm Petri dish containing 2 ml of MiR05 (0.5 mM EGTA, 3 mM $MgCl_2$, 60 mM lactobionic acid, 20 mM taurine, 10 mM KH_2PO_4, 20 mM HEPES, 110 mM sucrose, 1% BSA (pH 7.1 adjusted with 5 M KOH)) (43) and 5 mg/ml saponin; preliminary experiments showed that permeabilized islets demonstrated higher coupled respiration rates. Islets were gently rocked in the permeabilization medium for 20 min. After 20 min, the islets were rinsed with fresh MiR05 in the absence of saponin and then pipetted into an Oxygraph-2k chamber (Oroboros) containing 2 ml of air-equilibrated MiR05 at 37 °C. Oxygen electrodes were calibrated to air-saturated MiR05 buffer at 37 °C using published oxygen solubilities (44) corrected for local atmospheric pressure, and zero-oxygen calibrations were performed at regular intervals throughout the study. Oxygen concentration and oxygen flux were recorded using DatLab software (Oroboros). A modified substrate-uncoupler-inhibitor titration (SUIT) protocol based on Votion *et al.* (45) was applied. Respiratory flux through complex I was measured by adding 5 mM glutamate and 1 mM malate followed by 1.25 mM ADP to induce oxidative phosphorylation. To assess the integrity of the outer mitochondrial membrane, cytochrome *c* was added to the chamber (8 μM) (46), and no significant increases in respiration were observed. Convergent electron flow through complexes I and II was measured with the addition of 10 mM succinate, allowing the electron transport system to achieve maximal coupled respiration. Next, a stepwise addition of carbonyl cyanide *p*-trifluoro-methoxyphenyl hydrazone (FCCP) was used to completely uncouple mitochondria (0.25 μM initial + 0.25 μM

additions). To assess oxygen flux through complex II, 0.5 μM rotenone was added to inhibit complex I. Finally, electron transfer was blocked at complex III with the addition of 5 μM antimycin A and allowed to run long enough to obtain a residual oxygen consumption rate. Oxygen flux was expressed per mg of total protein (Pierce 660 nm protein assay, Thermo Fisher, 22660).

Glucose-stimulated insulin secretion

The glucose-stimulated insulin secretion assay was performed on mouse islets treated overnight with vehicle or CDK1 inhibitor, which were present throughout the assay. All experiments were carried out at 37 °C in a 5% CO_2 incubator using DMEM (Sigma, D-5030) containing 4 mM L-glutamine, 44 mM sodium bicarbonate, 10 mM HEPES, and 0.2% BSA. 60 islets per treatment were preincubated for 45 min in DMEM, 1.7 mM glucose, which was discarded. Six groups of 10 islets were then moved to 12-well plates (Falcon, 353225) containing 1 ml of DMEM, 1.7 mM glucose for 45 min. The islets were transferred to a new 12-well plate, each well containing 1 ml of DMEM, 16.7 mM glucose, for an additional 45-min incubation. The incubation medium was collected, and the islets were lysed in cell lysis buffer containing 20 mM Tris-HCl (pH 7.5), 150 mM NaCl, and 1% Triton X-100.

Insulin ELISA

Insulin secretion as a percentage of total islet insulin content was measured by ELISA in 96-well plates (Corning, 3096) coated overnight with 3 μg/ml (50 μl/well) anti-insulin primary antibody (Research Diagnostics, RDI-TRK2IP10-D6C4) diluted 1:2500 in PBS. Plates were blocked with PBS containing 4% BSA (Sigma, A7888) for 1 h (100 μl/well). Following blocking, plates were emptied and incubated for 1 h with either insulin standards (Millipore, 24304391/8013-k; 0.1–10 ng/ml), secretion medium, or islet lysate (25 μl/well). Secondary antibody (Research Diagnostics, RDI-TRK2IP10-D3E7-BT) (25 μl/well) diluted 1:1000 in PBS with 1% BSA was added to each well, gently mixed, and incubated for an additional hour. Wells were then washed three times (50 mM Tris, 0.2% Tween 20 (pH 8.0)), and 1 μg/ml streptavidin-horseradish peroxidase (Pierce, 21126) in PBS with 0.1% BSA was added (50 μl/well) and incubated for 30 min. Plates were then washed three times. 16 μmol/ml *o*-phenylenediamine (Sigma, P-5412), dissolved in citrate buffer (0.1 M citrate-phosphate, 0.03% H_2O_2 (pH 5.0)), was then added (50 μl/well). After 3–5 min of development, 0.18 M sulfuric acid (50 μl/well) was added to quench the reaction. Absorbance at 492 nm was determined by a plate reader (TECAN Infinite M1000 Pro). Insulin contents in plasma were calculated by comparison with known standards.

Quantitative PCR

Islets were isolated and washed with PBS. DNA was isolated with a Mini Genomic DNA kit (IBI Scientific). SYBR Green primers were designed using the Roche Universal Probe Library Assay Design Center tool. Quantitative PCR for mitochondrial DNA was performed in triplicate using primers MT9 (GAGCATCTTATCCACGCTTCC) and MT11 (GGTGGTACTCCCGCTGTAAA) normalized to reference gene *Ndufv1* (F, TTCCTCTGGATTCACCCTCA; R, CATGAGGAGCGCGAGTATTT) and *Ndufs3* (F, CGGCAGAACCGTTTTGAG; R, TCAATGGGTGTCAGCTCATC), *Ndufa9* (F, TTAGAGCGCTTCCAATGTCA; R, ATGGTGAAGCTGGCGATG), and *Atp5a1* (F, CCATGCCTCTAACACTCGAC; R, ACGTGTCAGCTCCCAGAA) with reference gene *Rplp0* (F, ACTGGTCTAGGACCCGAGAAG; R, TCCCACCTTGTCTCCAGTCT) for complex I expression analysis. FastStart Universal SYBR Green Master Rox (Roche Applied Science) was used with 30 ng of DNA per reaction with a final primer concentration of 2 μM. Total RNA was purified from isolated islets using the RNeasy Mini kit (Qiagen, 74104). First-strand cDNA was synthesized from purified RNA (150 ng) using the SuperScript III Synthesis System for RT-PCR (Invitrogen, 18080051). Real-time quantitative PCR was performed using SYBR Green–based detection (Applied Biosystems, 4367659) and the comparative CT method with *Rplp0* as the endogenous control on an Applied Biosystems QuantStudio 6 Flex System.

Statistics

Data are expressed as mean ± S.E. Statistical significance was determined using one- or two-way ANOVA with Sidak's multiple-comparisons post hoc test or Student's *t* test as appropriate. Differences were considered statistically significant at $p < 0.05$. Statistical calculations were performed with GraphPad Prism.

Author contributions—T. G. and M. J. M. conceptualization; T. G., S. M. S., J. W. R., and M. J. M. data curation; T. G., S. M. S., R. S. D., and M. J. M. formal analysis; T. G., S. M. S., and M. J. M. validation; T. G., S. M. S., R. S. D., J. W. R., and S. L. L. investigation; T. G., S. M. S., and M. J. M. visualization; T. G., S. M. S., J. W. R., S. L. L., and M. J. M. methodology; T. G. and M. J. M. writing-original draft; S. M. S. software; D. J. P., J. M. D., and M. J. M. resources; D. J. P., J. M. D., and M. J. M. supervision; J. M. D. and M. J. M. project administration; M. J. M. funding acquisition; M. J. M. writing-review and editing.

Acknowledgments—We thank Alan Attie for sharing the microarray study, Joshua Coon and Alex Hebert for assistance with phosphoproteomics, Brian Schmidt for assistance with glucose tolerance tests, Adam Jochem for assistance with cell fractionation, Elizabeth De Leon and Jamie Larmie for assistance with quantitative PCR, and Halena VanDeusen for preparing adenovirus. This work utilized facilities and resources from the William S. Middleton Memorial Veterans Hospital.

References

1. Bock, T., Pakkenberg, B., and Buschard, K. (2003) Increased islet volume but unchanged islet number in ob/ob mice. *Diabetes* **52,** 1716–1722 CrossRef Medline
2. Park, S.-H., Ryu, S.-Y., Yu, W.-J., Han, Y. E., Ji, Y.-S., Oh, K., Sohn, J.-W., Lim, A., Jeon, J.-P., Lee, H., Lee, K.-H., Lee, S.-H., Berggren, P.-O., Jeon, J.-H., and Ho, W.-K. (2013) Leptin promotes K(ATP) channel trafficking by AMPK signaling in pancreatic β-cells. *Proc. Natl. Acad. Sci. U.S.A.* **110,** 12673–12678 CrossRef Medline
3. Irles, E., Ñeco, P., Lluesma, M., Villar-Pazos, S., Santos-Silva, J. C., Vettorazzi, J. F., Alonso-Magdalena, P., Carneiro, E. M., Boschero, A. C., Nadal Á., Quesada, I. (2015) Enhanced glucose-induced intracellular signaling promotes insulin hypersecretion: pancreatic β-cell functional adaptations

in a model of genetic obesity and prediabetes. *Mol. Cell. Endocrinol.* **404,** 46–55 CrossRef Medline

4. van der Meulen, T., Donaldson, C. J., Cáceres, E., Hunter, A. E., Cowing-Zitron, C., Pound, L. D., Adams, M. W., Zembrzycki, A., Grove, K. L., and Huising, M. O. (2015) Urocortin3 mediates somatostatin-dependent negative feedback control of insulin secretion. *Nat. Med.* **21,** 769–776 CrossRef Medline
5. Keller, M. P., Choi, Y., Wang, P., Davis, D. B., Rabaglia, M. E., Oler, A. T., Stapleton, D. S., Argmann, C., Schueler, K. L., Edwards, S., Steinberg, H. A., Chaibub Neto, E., Kleinhanz, R., Turner, S., Hellerstein, M. K., *et al.* (2008) A gene expression network model of type 2 diabetes links cell cycle regulation in islets with diabetes susceptibility. *Genome Res.* **18,** 706–716 CrossRef Medline
6. Gavet, O., and Pines, J. (2010) Activation of cyclin B1-Cdk1 synchronizes events in the nucleus and the cytoplasm at mitosis. *J. Cell Biol.* **189,** 247–259 CrossRef Medline
7. Dephoure, N., Zhou, C., Villén, J., Beausoleil, S. A., Bakalarski, C. E., Elledge, S. J., and Gygi, S. P. (2008) A quantitative atlas of mitotic phosphorylation. *Proc. Natl. Acad. Sci. U.S.A.* **105,** 10762–10767 CrossRef Medline
8. Wang, Z., Fan, M., Candas, D., Zhang, T.-Q., Qin, L., Eldridge, A., Wachsmann-Hogiu, S., Ahmed, K. M., Chromy, B. A., Nantajit, D., Duru, N., He, F., Chen, M., Finkel, T., Weinstein, L. S., *et al.* (2014) Cyclin B1/Cdk1 coordinates mitochondrial respiration for cell-cycle G2/M progression. *Dev. Cell* **29,** 217–232 CrossRef Medline
9. Prentki, M., Matschinsky, F. M., and Madiraju, S. R. (2013) Metabolic signaling in fuel-induced insulin secretion. *Cell Metab.* **18,** 162–185 CrossRef Medline
10. MacDonald, M. J. (1981) High content of mitochondrial glycerol-3-phosphate dehydrogenase in pancreatic islets and its inhibition by diazoxide. *J. Biol. Chem.* **256,** 8287–8290 Medline
11. Zhao, C., Wilson, M. C., Schuit, F., Halestrap, A. P., and Rutter, G. A. (2001) Expression and distribution of lactate/monocarboxylate transporter isoforms in pancreatic islets and the exocrine pancreas. *Diabetes* **50,** 361–366 CrossRef Medline
12. Schuit, F., De Vos, A., Farfari, S., Moens, K., Pipeleers, D., Brun, T., and Prentki, M. (1997) Metabolic fate of glucose in purified islet cells. Glucose-regulated anaplerosis in β cells. *J. Biol. Chem.* **272,** 18572–18579 CrossRef Medline
13. Vassilev, L. T., Tovar, C., Chen, S., Knezevic, D., Zhao, X., Sun, H., Heimbrook, D. C., and Chen, L. (2006) Selective small-molecule inhibitor reveals critical mitotic functions of human CDK1. *Proc. Natl. Acad. Sci. U.S.A.* **103,** 10660–10665 CrossRef Medline
14. Jorda, R., Hendrychová, D., Voller, J., Řezníčková, E., Gucký, T., and Kryštof, V. (2018) How selective are pharmacological inhibitors of cell-cycle-regulating cyclin-dependent kinases? *J. Med. Chem.* **61,** 9105–9120 CrossRef Medline
15. Qin, L., Fan, M., Candas, D., Jiang, G., Papadopoulos, S., Tian, L., Woloschak, G., Grdina, D. J., and Li, J. J. (2015) CDK1 enhances mitochondrial bioenergetics for radiation-induced DNA repair. *Cell Rep.* **13,** 2056–2063 CrossRef Medline
16. Veas-Pérez de Tudela, M., Delgado-Esteban, M., Maestre, C., Bobo-Jiménez, V., Jiménez-Blasco, D., Vecino, R., Bolaños, J. P., and Almeida, A. (2015) Regulation of Bcl-xL-ATP synthase interaction by mitochondrial cyclin B1-cyclin-dependent kinase-1 determines neuronal survival. *J. Neurosci.* **35,** 9287–9301 CrossRef Medline
17. Li, H.-B., Wang, R.-X., Jiang, H.-B., Zhang, E.-D., Tan, J.-Q., Xu, H.-Z., Zhou, R.-R., and Xia, X.-B. (2016) Mitochondrial ribosomal protein L10 associates with cyclin B1/Cdk1 activity and mitochondrial function. *DNA Cell Biol.* **35,** 680–690 CrossRef Medline
18. Gregg, T., Poudel, C., Schmidt, B. A., Dhillon, R. S., Sdao, S. M., Truchan, N. A., Baar, E. L., Fernandez, L. A., Denu, J. M., Eliceiri, K. W., Rogers, J. D., Kimple, M. E., Lamming, D. W., and Merrins, M. J. (2016) Pancreatic β-cells from mice offset age-associated mitochondrial deficiency with reduced K_{ATP} channel activity. *Diabetes* **65,** 2700–2710 CrossRef Medline
19. Lakowicz, J. R., Szmacinski, H., Nowaczyk, K., and Johnson, M. L. (1992) Fluorescence lifetime imaging of free and protein-bound NADH. *Proc. Natl. Acad. Sci. U.S.A.* **89,** 1271–1275 CrossRef Medline
20. Blinova, K., Carroll, S., Bose, S., Smirnov, A. V., Harvey, J. J., Knutson, J. R., and Balaban, R. S. (2005) Distribution of mitochondrial NADH fluorescence lifetimes: steady-state kinetics of matrix NADH interactions. *Biochemistry* **44,** 2585–2594 CrossRef Medline
21. Blinova, K., Levine, R. L., Boja, E. S., Griffiths, G. L., Shi, Z.-D., Ruddy, B., and Balaban, R. S. (2008) Mitochondrial NADH fluorescence is enhanced by complex I binding. *Biochemistry* **47,** 9636–9645 CrossRef Medline
22. Digman, M. A., Caiolfa, V. R., Zamai, M., and Gratton, E. (2008) The phasor approach to fluorescence lifetime imaging analysis. *Biophys. J.* **94,** L14–16 CrossRef Medline
23. Farfari, S., Schulz, V., Corkey, B., and Prentki, M. (2000) Glucose-regulated anaplerosis and cataplerosis in pancreatic β-cells: possible implication of a pyruvate/citrate shuttle in insulin secretion. *Diabetes* **49,** 718–726 CrossRef Medline
24. Joseph, J. W., Jensen, M. V., Ilkayeva, O., Palmieri, F., Alárcon, C., Rhodes, C. J., and Newgard, C. B. (2006) The mitochondrial citrate/isocitrate carrier plays a regulatory role in glucose-stimulated insulin secretion. *J. Biol. Chem.* **281,** 35624–35632 CrossRef Medline
25. Ferdaoussi, M., Dai, X., Jensen, M. V., Wang, R., Peterson, B. S., Huang, C., Ilkayeva, O., Smith, N., Miller, N., Hajmrle, C., Spigelman, A. F., Wright, R. C., Plummer, G., Suzuki, K., Mackay, J. P., *et al.* (2015) Isocitrate-to-SENP1 signaling amplifies insulin secretion and rescues dysfunctional β cells. *J. Clin. Investig.* **125,** 3847–3860 CrossRef Medline
26. Alves, T. C., Pongratz, R. L., Zhao, X., Yarborough, O., Sereda, S., Shirihai, O., Cline, G. W., Mason, G., and Kibbey, R. G. (2015) Integrated, step-wise, mass-isotopomeric flux analysis of the TCA cycle. *Cell Metab.* **22,** 936–947 CrossRef Medline
27. Ewald, J. C., Reich, S., Baumann, S., Frommer, W. B., and Zamboni, N. (2011) Engineering genetically encoded nanosensors for real-time *in vivo* measurements of citrate concentrations. *PLoS One* **6,** e28245 CrossRef Medline
28. Ravier, M. A., Daro, D., Roma, L. P., Jonas, J.-C., Cheng-Xue, R., Schuit, F. C., and Gilon, P. (2011) Mechanisms of control of the free Ca^{2+} concentration in the endoplasmic reticulum of mouse pancreatic β-cells: interplay with cell metabolism and $[Ca^{2+}]_c$ and role of SERCA2b and SERCA3. *Diabetes* **60,** 2533–2545 CrossRef Medline
29. Miura, R. M., and Pernarowski, M. (1995) Correlations of rates of insulin release from islets and plateau fractions for β-cells. *Bull. Math. Biol.* **57,** 229–246 CrossRef Medline
30. Henquin, J. C. (2009) Regulation of insulin secretion: a matter of phase control and amplitude modulation. *Diabetologia* **52,** 739–751 CrossRef Medline
31. Nicholls, D. G. (2016) The pancreatic β-cell: a bioenergetic perspective. *Physiol. Rev.* **96,** 1385–1447 CrossRef Medline
32. Affourtit, C., Alberts, B., Barlow, J., Carré, J. E., and Wynne, A. G. (2018) Control of pancreatic β-cell bioenergetics. *Biochem. Soc. Trans.* **46,** 555–564 CrossRef Medline
33. Sekine, N., Cirulli, V., Regazzi, R., Brown, L. J., Gine, E., Tamarit-Rodriguez, J., Girotti, M., Marie, S., MacDonald, M. J., and Wollheim, C. B. (1994) Low lactate dehydrogenase and high mitochondrial glycerol phosphate dehydrogenase in pancreatic beta-cells. Potential role in nutrient sensing. *J. Biol. Chem.* **269,** 4895–4902 Medline
34. Stark, R., Pasquel, F., Turcu, A., Pongratz, R. L., Roden, M., Cline, G. W., Shulman, G. I., and Kibbey, R. G. (2009) Phosphoenolpyruvate cycling via mitochondrial phosphoenolpyruvate carboxykinase links anaplerosis and mitochondrial GTP with insulin secretion. *J. Biol. Chem.* **284,** 26578–26590 CrossRef Medline
35. Shirakawa, J., Fernandez, M., Takatani, T., El Ouaamari, A., Jungtrakoon, P., Okawa, E. R., Zhang, W., Yi, P., Doria, A., and Kulkarni, R. N. (2017) Insulin signaling regulates the FoxM1/PLK1/CENP-A pathway to promote adaptive pancreatic β cell proliferation. *Cell Metab.* **25,** 868–882.e5 CrossRef Medline
36. Diril, M. K., Ratnacaram, C. K., Padmakumar, V. C., Du, T., Wasser, M., Coppola, V., Tessarollo, L., and Kaldis, P. (2012) Cyclin-dependent kinase 1 (Cdk1) is essential for cell division and suppression of DNA re-replication but not for liver regeneration. *Proc. Natl. Acad. Sci. U.S.A.* **109,** 3826–3831 CrossRef Medline

37. Thorens, B., Tarussio, D., Maestro, M. A., Rovira, M., Heikkilä, E., and Ferrer, J. (2015) Ins1(Cre) knock-in mice for β cell-specific gene recombination. *Diabetologia* **58,** 558–565 CrossRef Medline
38. Kang, C., Xie, L., Gunasekar, S. K., Mishra, A., Zhang, Y., Pai, S., Gao, Y., Kumar, A., Norris, A. W., Stephens, S. B., and Sah, R. (2018) SWELL1 is a glucose sensor regulating β-cell excitability and systemic glycaemia. *Nat. Commun.* **9,** 367 CrossRef Medline
39. Annicotte, J.-S., Blanchet, E., Chavey, C., Iankova, I., Costes, S., Assou, S., Teyssier, J., Dalle, S., Sardet, C., and Fajas, L. (2009) The CDK4-pRB-E2F1 pathway controls insulin secretion. *Nat. Cell Biol.* **11,** 1017–1023 CrossRef Medline
40. Kim, S. Y., Lee, J.-H., Merrins, M. J., Gavrilova, O., Bisteau, X., Kaldis, P., Satin, L. S., and Rane, S. G. (2017) Loss of cyclin-dependent kinase 2 in the pancreas links primary β-cell dysfunction to progressive depletion of β-cell mass and diabetes. *J. Biol. Chem.* **292,** 3841–3853 CrossRef Medline
41. Solaki, M., and Ewald, J. C. (2018) Fueling the cycle: CDKs in carbon and energy metabolism. *Front. Cell Dev. Biol.* **6,** 93 CrossRef Medline
42. Merrins, M. J., Van Dyke, A. R., Mapp, A. K., Rizzo, M. A., and Satin, L. S. (2013) Direct measurements of oscillatory glycolysis in pancreatic islet β-cells using novel fluorescence resonance energy transfer (FRET) biosensors for pyruvate kinase M2 activity. *J. Biol. Chem.* **288,** 33312–33322 CrossRef Medline
43. Gnaiger, E., and Kuznetsov, A. V. (2002) Mitochondrial respiration at low levels of oxygen and cytochrome c. *Biochem. Soc. Trans.* **30,** 252–258 CrossRef Medline
44. Forstner, H., and Gnaiger, E. (1983) Calculation of equilibrium oxygen concentration, in *Polarographic Oxygen Sensors* (Gnaiger, E., and Forstner, H., eds) pp. 321–333, Springer, New York
45. Votion, D.-M., Gnaiger, E., Lemieux, H., Mouithys-Mickalad, A., and Serteyn, D. (2012) Physical fitness and mitochondrial respiratory capacity in horse skeletal muscle. *PLoS One* **7,** e34890 CrossRef Medline
46. Kuznetsov, A. V., Schneeberger, S., Seiler, R., Brandacher, G., Mark, W., Steurer, W., Saks, V., Usson, Y., Margreiter, R., and Gnaiger, E. (2004) Mitochondrial defects and heterogeneous cytochrome c release after cardiac cold ischemia and reperfusion. *Am. J. Physiol. Heart Circ. Physiol.* **286,** H1633–H1641 CrossRef Medline